

5-3. Contract Beamlines

BL22XU JAEA Actinide Science I

1. Introduction

BL22XU is designed to promote basic and applied research on nuclear energy, Fukushima environmental recovery research, decommissioning research, and related research. It was constructed in the Storage Ring and the RI Laboratory of SPring-8 to investigate radioactive materials containing transuranium elements.

BL22XU have two double-crystal monochromators; one is a single cam-type monochromator with the multi-crystal switching system^[1]. This monochromator can utilize wide-energy-range X-rays from 4 to 72 keV by using Si(111) and Si(311) crystals. The other is a calculation- and combination-type monochromator. This monochromator can utilize high-flux X-rays from 35 to 70 keV by using Si(111) crystals.

After repairing the multi-element SSD detector, we are preparing for the microanalysis of various radioactive materials in combination with the KB mirror.

2. Experimental hutch 1 (EH1)

2-1. Diamond anvil-cell diffractometer

The diamond anvil-cell diffractometer is designed for both single-crystal and powder X-ray diffraction experiments under high pressure and low temperature. Equipped large-area two-dimensional detectors enable us to measure X-ray scattering patterns even at a high-Q range with a short exposure time. By using these detectors and high-energy monochromatic X-rays

of 50–70 keV, this diffractometer is also used for X-ray total scattering measurements to obtain the pair-distribution function (PDF).

The demand for PDF measurements has steadily increased because the structural information of functional materials in local to middle-range structures has been regarded as important for understanding their properties. Our PDF system has been applied to a wide variety of functional materials, such as hydrogen-absorbing alloys^[2,3], negative thermal expansion materials^[4], and cement materials^[5]. Recently, our system has succeeded in obtaining PDFs of the highly textured Mg-Ti thin film and has revealed the presence of Ti clusters in the Mg matrix^[2].

The gas-loading apparatus and N₂ gas flow device enable us to measure X-ray total scattering patterns under H₂ gas pressure below 1 MPa and temperature of 100–400 K. Usually, a polyimide tube with an outer diameter of 1.1 mm is used as the sample container. The new attachments holding the sample container were introduced to be able to use other tubes, such as tubes with outer diameters of 0.55, 0.7, and 2.0 mm.

2-2. Large diffractometer

Currently, an apparatus for Bragg coherent X-ray diffraction imaging (Bragg-CDI) is under development^[6]. Bragg-CDI is expected to be a powerful technique for investigating an individual nanosized crystalline particle and should enable studies of particles located within devices, which

are inaccessible by electron beam techniques. This technique was used to study particles as small as ~100 nm in size, which is the most interesting size.

In 2020, we expanded the applicable particle size to 40–500 nm^[7]. A vacuum environment prepared around the sample enabled us to obtain a high-contrast diffraction pattern from a 40 nm particle. The reconstructed three-dimensional image showed the outer shape, size, and internal strain for a single particle. A single 500 nm BaTiO₃ particle showed a straight and sharp antiphase-boundary shape, whereas smaller BaTiO₃ particles showed different phase boundary shapes.

Rod-shaped scattering has been observed in the tetragonal phase of Pb(Mg_{1/3}Nb_{2/3})O₃–28.7%PbTiO₃ by using the backscattering setting^[8]. We attribute it to the crystal truncation rod (CTR) scattering associated with the boundary of 90° domains. The CTR scattering shows a characteristic temperature evolution, which enables us to discuss the properties of domain walls, especially their temperature dependence on the domain wall width. Although it is necessary to have a situation where the crystal coherence is suddenly truncated, similarly to the 90° domain wall, the CTR scattering can be expected to be a powerful tool for examining the domain wall properties.

3. Experimental hutch 3 (EH3)

3-1. Hard X-ray photoemission spectroscopy (HAXPES)

A feature of the HAXPES analyzer at BL22XU is the angle-resolved analysis using a wide-angle acceptance object lens with a photoelectron acceptance of ± 30 degrees. In FY2020, a

Kirkpatrick-Baez (KB) micro-focusing system was introduced to the HAXPES station. It can precisely measure the chemical bonding state in a three-dimensional microdomain at a buried interface in combination with a micro-focused SR beam by the KB mirror.

HAXPES measurements have been performed to estimate the radiation damage effect of bilayer samples of Pt/Y₃Fe₅O₁₂ (Pt/YIG), which shows the spin Seebeck effect. Unlike the normal Seebeck effect, which uses charge degrees of freedom, the spin Seebeck effect uses spin degrees of freedom for thermoelectric generation, and the devices using the spin Seebeck effect generally have a strong tolerance to irradiation damage such as lattice defects^[9]. Therefore, the use of vitrified waste from nuclear power plants as an energy resource is expected. Last year, it was reported that during HAXPES measurements, Pt/YIG samples irradiated with 320 MeV gold ion (Au²⁴⁺) beams were damaged probably because of the chemical reaction at the interface between Pt and YIG^[10]. This year, we observed the electronic state of a Pt/YIG sample irradiated with steam up to 150 °C and/or 1.1 MeV γ -rays of ⁶⁰Co. The same effect as that of the gold-ion-irradiated samples was observed, and more detailed analyses and measurements are ongoing.

3-2. X-ray absorption fine structure (XAFS)

(1) XAFS study on simulated fuel debris

For the decommissioning of the Fukushima-Daiichi Nuclear Power Plant, it is necessary to understand the characteristics of fuel debris. In particular, for the safe and reliable removal of the debris, the estimation of the aged deterioration of the debris with changes in

environmental conditions is required. Thus, in this study, we aim to investigate the changes in the chemical state and structure of simulated fuel debris under a controlled atmosphere by the XAFS method.

Fuel debris is considered to be immersed in water under reductive and high radiation conditions. If the debris is removed from the reactor, it will be exposed to an oxidative atmosphere, which can cause the characteristic changes. Thus, to simulate such conditions, we prepared simulated fuel debris that was immersed in water and irradiated with γ -rays, and measured the U-LIII edge XAFS of the sample before and after it was picked up from the water and exposed to air. As a result, it was revealed that uranium was

oxidized by gamma irradiation and continuous water immersion, and that the U-O bond distance became shorter with the oxidation (Fig. 1). At this time, uranium hardly eluted into the water. Furthermore, both the valence and local structure of uranium hardly changed even when the samples were exposed to air, suggesting that the debris is stable under air ambient.

(2) XAFS spectra for radium (Ra) at L_{III}-edge

Radium (Ra) is an important radioactive element in terms of environmental pollution around a uranium mine and the geological disposal of radioactive waste. In addition, the higher concentration of Ra in drinking water than the regulation value due to natural Ra without an anthropogenic effect was reported [11], indicating that the environmental behavior of Ra should be urgently investigated.

Clay minerals play an important role in the environmental behavior of Ra [12]. Ions adsorbed on clay minerals generally have a completely different environmental behavior depending on the adsorption structures, namely, the formation of inner- or outer-sphere complexes. Therefore, whether Ra forms an inner- or outer-sphere complex on clay minerals should be clarified. However, even the hydration structure of Ra has not been investigated at the molecular level, which is related to the formation of the outer-sphere complex adsorbed as hydrated ion. Therefore, our purpose in this study is to investigate the hydration and adsorption structures of Ra on clay minerals using the extended X-ray absorption fine structure (EXAFS).

The hydrated Ra²⁺ and Ra²⁺-adsorbed clay samples for EXAFS were prepared using a Ra²⁺ aqueous solution purified in Osaka University

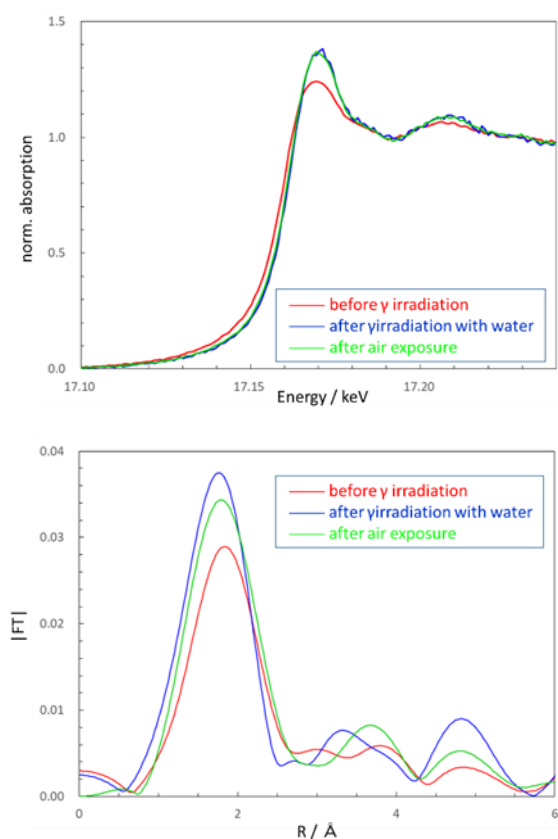


Fig. 1. XANES spectra (upper) and radial structure functions (lower) of simulated fuel debris under several conditions.

following the regulation guidelines. As for the clay minerals, vermiculite and montmorillonite were used. EXAFS spectra were collected at BL22XU in SPring-8. The hydration structures of Ra and barium (Ba), which is an analog element, were also investigated by *ab initio* molecular dynamics.

The coordination number and distance between Ra and oxygen (O) in the first hydration shell obtained by EXAFS method were consistent with those obtained by simulation. The distance between Ra and O was about 1.4 Å larger than the effective ionic radius of Ra^{2+} , which is identical to those of other alkali earth metal ions. The EXAFS results suggested that Ra forms inner- or outer-sphere complexes on vermiculite or montmorillonite, respectively. These results suggest that the environmental behavior of Ra is controlled by fixation on vermiculite and other phyllosilicates.

(3) Development of fluorescence XAFS imaging using pinhole camera

We attempted to develop a fluorescence imaging XAFS method for the fast screening of transition metal elements with low-energy X-ray absorption edges and their valence distribution in the samples such as glass materials, which are difficult to make thin and use in a transmission method. To obtain XAFS spectra with high sensitivity and positional resolution, a direct imaging detector without a scintillator and a pinhole were used. The results were demonstrated with a highly brilliant synchrotron radiation undulator X-ray with variable incident energy [13].

Ce L3 absorption edge fluorescence imaging XAFS measurements were performed by detecting Ce L α lines from 5.69 to 5.79 keV in 1 eV steps,

with a dwell time of 40 s per energy as shown in Fig. 2. A 50 μm tungsten pinhole was used. The direct imaging CCD detector had 1024×1024 pixels, a pixel size of 13 μm , and a field of view of 13.3×13.3 mm. An area of 2×2 pixels was binned for the measurement in Fig. 2. An X-ray beam of 2 mm (length) \times 3 mm (width) was irradiated onto a sample plate tilted by 1 degree. CePO_4 and CeO_2 mixtures were measured. A double-sided tape was attached to the glass slide and the sample was placed on it. The X-rays were irradiated from the right side of the figure, showing that CePO_4 has a finer particle size and is more evenly distributed, whereas CeO_2 has a coarser particle size and black voids where there is no fluorescence from the sample. A linear combination analysis was performed on the fluorescence imaging XAFS results of the mixed samples using the acquired standard data. The results were well fitted, and the mixed sample was found to be composed of 40% CePO_4 and 60% CeO_2 .

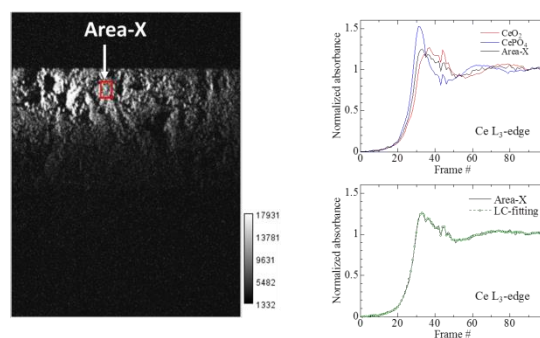


Fig. 2. Fluorescence X-ray image at Ce L3 absorption edge at 5.85 keV (left) and imaging XAFS spectra (right).

(4) Structural analyses of complex formed in adsorbent for MA(III) recovery

Japan Atomic Energy Agency has been developing

recovery of trivalent minor actinides (MA(III): Am and Cm) from spent nuclear fuel for reductions in the volume and radiotoxicity of highly active liquid wastes. MA(III) in the liquid wastes are recovered by adsorption/elution reaction with a ligand impregnating into the porous silica-based adsorbents. Currently, the performance of the adsorbent is improved by optimizing the structure of the ligand. In this study, two nitrilotriacetic (NTA) amides were employed for the ligand, and the performance of the adsorbents and the local structure of complexes formed in the adsorbents were investigated.

A rare-earth element (Nd, Sm or Eu) was loaded into porous silica-based adsorbents impregnating N,N,N',N',N'',N'''-hexa-octyl-nitrilotriacetamide (HONTA) or N,N,N',N',N'',N'''-hexa-2-ethylhexyl-nitrilotriacetamide (H2EHNTA) from a nitric acid medium, and the local structure around the rare-earth elements was investigated by K-edge EXAFS measurements in the transmission mode.

The adsorption performance of rare-earth elements depends on the acidity of the nitric acid, and the adsorption ratio decreases with increasing acidity for both adsorbents. The H2EHNTA adsorbent showed slightly better adsorption performance of the rare-earth elements, and the HONTA adsorbent might have an advantage for

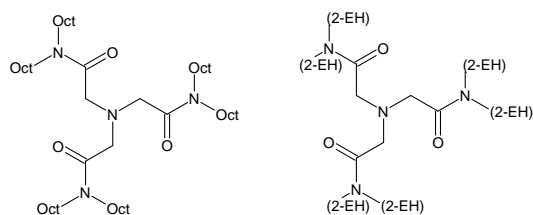


Fig. 3. NTA amides: HONTA (left) and H2EHNTA (right).

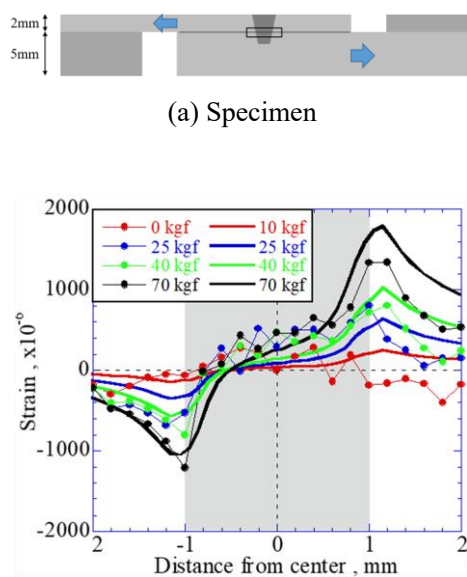
selective MA(III) adsorption.

The number of nearest neighboring O atoms around rare-earth elements evaluated by EXAFS also showed dependence on the ligand. The coordination number of the HONTA system was slightly larger than that of the H2EHNTA system. The branched side chain of the NTA amides may affect the coordination of the nitrate ion inside the cross-linked polymer in the adsorbent. Currently, the structural analysis of complexes of the system in which rare-earth elements coexist is underway.

3-3. Stress/imaging measurements

In this device, deformation and state changes inside a material are determined by a diffraction method and an imaging method using high-energy synchrotron radiation X-rays. Figure 4 shows the specimen and strain distribution under loading^[14]. The X-ray energy was 70.11 keV. PNC-FMS, which holds promise for the internal ducts of next-generation nuclear reactors, was used as the test material. Two specimens with dimensions of $70 \times 6 \times 2$ and $70 \times 6 \times 5$ mm were overlapped, and an Yb fiber laser with a power of 1.3 kW and a heat input of 1500 J was irradiated and joined the two specimens from the 2-mm-thick plate side. The sub-interface strain (Fig. 4(b)) in the square frame near the interface in Fig. 4(a) shows a symmetrical distribution under loading. The measured and finite element method (FEM) results agreed qualitatively. For example, a change in tensile or compressive strain altered the strain in the weld. However, the change slightly differed quantitatively. The measured strain left of the center was larger than the theoretical strain, whereas that on the right was smaller than the theoretical strain. The existence of internal

defects is considered to be one of the causes of the difference between the experimental and theoretical results. When we measured the transmission image from the side of the specimen using synchrotron radiation X-rays, we found that the molten portion contained multiple voids and cracks. In the future, if the positions of such defects are clarified three dimensionally, more accurate strain predictions will be possible.



(b) Strain distribution under the interface by FEM and measurements.

Fig. 4. Specimen and strain distribution.

3-4. K-type diffractometer

We are studying an evaluation method for a sample in which crystals and glass are mixed in preparation for the upcoming evaluation of actual debris.

The X-ray diffraction pattern of the oxide ferroelectric $\text{Bi}_{0.5}\text{Na}_{0.5}\text{TiO}_3$ (BNT) is composed of Bragg reflection and diffuse scattering. Figure 5 shows the result of fitting the PDF analysis of BNT with the average structure obtained by using Bragg

reflection. The differences fitted in the mean structure were found to be consistent with the PDF using only diffuse scattering [15].

As a result, it was found that accurate data that does not hinder the analysis even for weak diffuse scattering compared with Bragg reflection can be obtained.

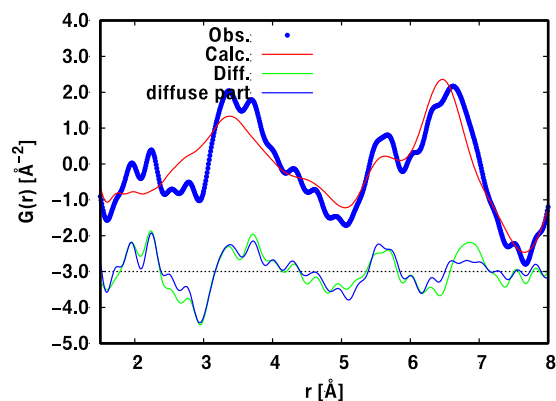


Fig. 5. Difference PDF when fitting with the average structure of $\text{Bi}_{0.5}\text{Na}_{0.5}\text{TiO}_3$ and PDF of diffuse components.

Hideaki Shiwaku^{*1}, Akihiko Machida^{*2}, Kenji Ohwada^{*2}, Masaaki Kobata^{*1}, Tatsuo Fukuda^{*1}, Hajime Tanida^{*1}, Tohru Kobayashi^{*1}, Eiko Yamaguchi^{*1}, Sou Watanabe^{*1}, Haruaki Matsuura^{*3}, Takahisa Shobu^{*1}, and Yasuhiro Yoneda^{*1}

^{*1}Japan Atomic Energy Agency

^{*2}National Institutes for Quantum and Radiological Science and Technology

^{*3}Tokyo City University

References:

- [1] Shiwaku, H. et al. (2004). *AIP Conf. Proc.* **705**, 659.
- [2] Kim, H. et al. (2020). *Inorg. Chem.* **59**, 6800.
- [3] Nygård, M. M. et al. (2020). *Acta Mater.* **205**, 116496.
- [4] Nishikubo, T. et al. (2021). *Chem. Mater.* **33**,

- 1498.
- [5] Jee, H. et al. (2020). *J. Am. Ceram. Soc.* **103**, 7188.
 - [6] Ohwada, K. et al. (2019). *Jpn. J. Appl. Phys.* **58**, SLLA05.
 - [7] Oshime, N. et al. (2021). *Jpn. J. Appl. Phys.* **60**, SFFA07.
 - [8] Ohwada, K. et al. (2021). *Jpn. J. Appl. Phys.* **60**, SFFA05.
 - [9] Yagmur, A. et al. (2016). *Appl. Phys. Lett.* **109**, 243902.
 - [10] Okayasu, S. et al. (2020). *J. Appl. Phys.* **128**, 083902.
 - [11] Szabo, Z. dePaul, V. T. Fischer, J. M. Kraemer, T. F. & Jacobsen, E. (2012). *Appl. Geochem.* **27**, 729–752.
 - [12] Hidaka, H. Horie, K. & Gauthier-Lafaye, F. (2007). *Earth Planet. Sci. Lett.* **264**, 167–176.
 - [13] Tanida, H. & Okamoto, Y. (2021). *Adv. X-ray Anal.* **52**, 69–80.
 - [14] Shobu, T. et al. (2021). *Quantum Beam Sci.* **5**, 17.
 - [15] Yoneda, Y. & Noguchi, Y. to be published in *Jpn. J. Appl. Phys.*